Geophysical Research Letters

RESEARCH LETTER
10.1029/2023GL102785

Sources and Pathways of Glacial Meltwater in the Bellingshausen Sea, Antarctica

Peter M. F. Sheehan[1], Karen J. Heywood[1], Andrew F. Thompson[2], M. Mar Flexas[2], and Michael P. Schodlok[3]

[1]Centre for Ocean and Atmospheric Sciences, School of Environmental Sciences, University of East Anglia, Norwich, UK, [2]Environmental Science and Engineering, California Institute of Technology, Pasadena, CA, USA, [3]Jet Propulsion Laboratory, California Institute of Technology, Pasadena, CA, USA

Key Points:

- Meltwater pathways in the Bellingshausen Sea, Antarctica, are explored using observations from gliders and a high-resolution regional model
- Meltwater observed at different densities originates from different ice shelves: lighter meltwater layers originate from eastern ice shelves
- Meltwater from different ice shelves is distinguished by different turbidity signatures, suggestive of different biogeochemical properties

Supporting Information:

Supporting Information may be found in the online version of this article.

Correspondence to:

P. M. F. Sheehan,
p.sheehan@uea.ac.uk

Citation:

Sheehan, P. M. F., Heywood, K. J., Thompson, A. F., Flexas, M. M., & Schodlok, M. P. (2023). Sources and pathways of glacial meltwater in the Bellingshausen Sea, Antarctica. *Geophysical Research Letters*, *50*, e2023GL102785. https://doi.org/10.1029/2023GL102785

Received 6 JAN 2023
Accepted 1 JUL 2023

Abstract Meltwater content and pathways determine the impact of Antarctica's melting ice shelves on ocean circulation and climate. Using ocean glider observations, we quantify meltwater distribution and transport within the Bellingshausen Sea's Belgica Trough. Meltwater is present at different densities and with different turbidities: both are indicative of a layer's ice shelf of origin. To investigate how ice-shelf origin separates meltwater into different export pathways, we compare these observations with high-resolution tracer-release model simulations. Meltwater filaments branch off the Antarctic Coastal Current into the southwestern trough. Meltwater also enters the Belgica Trough in the northwest via an extended western pathway, hence the greater observed southward (0.50 mSv) than northward (0.17 mSv) meltwater transport. Together, the observations and simulations reveal meltwater retention within a cyclonic in-trough gyre, which has the potential to promote climactically important feedbacks on circulation and future melting.

Plain Language Summary Recent research has advanced our understanding of interactions between warm ocean waters and the underside of Antarctica's floating ice shelves. But what happens to meltwater that these ice shelves release? Meltwater is fresh: it reduces the salinity of sea water and upsets the delicate balance between salty and fresh water that drives many polar ocean processes - for example, the sinking of cold, salty water to the deepest regions of the ocean, which is of global climatic importance. We use high-resolution observations and state-of-the-art model simulations to determine the pathways that meltwater takes as it flows in and around the Belgica Trough in the central Bellingshausen Sea, Antarctica. Meltwater is principally confined to the edges of the trough's clockwise gyre circulation. Meltwater from eastern ice shelves is generally found at shallower depths than meltwater from southern ice shelves; this explains evidence of two meltwater layers found in our observations. In addition, meltwater from eastern ice shelves is turbid, while meltwater from southern ice shelves is clear. These results will help us to better predict how Antarctica's coastal seas will respond to a warming climate as ever more meltwater is released into the ocean.

1. Introduction

The intrusion of warm Modified Circumpolar Deep Water (mCDW; ~1.2°C, ~34.6 g kg^{-1}; Whitworth et al., 1998) onto the continental shelf of West Antarctica—that is, along the western coast of the Antarctic Peninsula and in the Bellingshausen and Amundsen Seas (Figure 1a)—contributes to melting of the region's glaciers and ice shelves (Jenkins et al., 2018; Wåhlin et al., 2010). Aided by the proximity of the Antarctic Circumpolar Current to the shelf break (Orsi et al., 1995), ocean and atmospheric processes control the delivery of mCDW to the ice front (e.g., Gunn et al., 2018; Kim et al., 2021; Kimura et al., 2017; Moffat et al., 2009; Nakayama et al., 2018; Oelerich et al., 2022). Widespread mCDW intrusions make sea floor temperatures over West Antarctica's continental shelf the warmest of all Antarctica's shelf seas (Thompson et al., 2018); the glaciers and ice shelves that meet these warm waters are the fastest melting on the continent (Rignot et al., 2019).

Glacial meltwater (i.e., fresh water derived from basal melting of ice shelves; "meltwater" hereafter) from mCDW-induced basal melting is injected at depth, but can rise to the surface if sufficiently buoyant given local stratification (Zheng et al., 2021). Meltwater can circle the continent (Nakayama et al., 2020) and modify ocean stratification, thus altering geostrophic circulation, vertical mixing and vertical and lateral heat fluxes. Transport of meltwater to deep-water formation sites, such as the Ross Sea, can alter the properties and formation rates of water masses that ventilate the abyssal ocean (Jacobs & Giulivi, 2010; Lago & England, 2019; Silvano

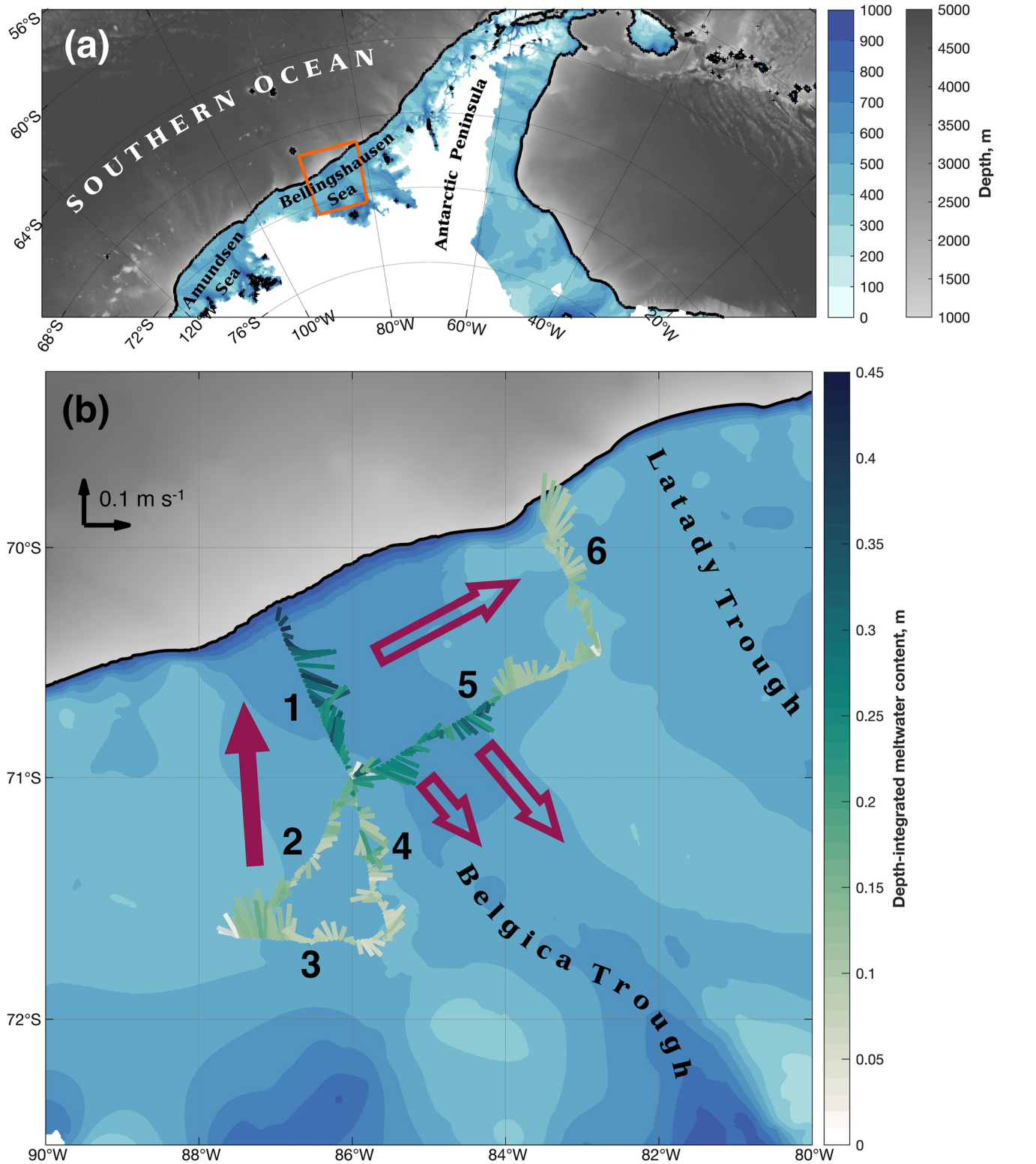

Figure 1. (a) Bathymetric map of the Southern Ocean and Antarctic continental shelf in the region of the Antarctic Peninsula, with the region shown in panel (b) outlined in orange. (b) Dive-average currents (m s^{-1}; key in top left) colored by depth-integrated meltwater content (m). Bathymetric shading is as in panel (a). Bold numbers indicate transect number and purple arrows approximate key flows based on dive-average currents; filled arrows indicate turbid flows, un-filled arrows indicate clear flows. In both panels, the 1,000 m isobath is indicated by the thick black line. Bathymetry is from RTopo-2.

et al., 2018). Circulation and stratification changes induced by the addition of meltwater can alter ice-shelf melt rates (Donat-Magnin et al., 2017; Flexas et al., 2022), even if the meltwater injection occurs far from the ice shelf. Quantifying meltwater content over the Antarctic continental shelf, and describing its pathways and origins, is therefore key to understanding the impact of a warming, melting Antarctica on ocean circulation.

The Bellingshausen Sea is poorly observed, general features of the circulation having been elucidated only recently and with sparse observations (e.g., Jenkins & Jacobs, 2008; Ruan et al., 2021; Schulze Chretien et al., 2021; Thompson et al., 2020; Zhang et al., 2016). Two major troughs are present: Belgica Trough in the west and Latady Trough in the east (Figure 1b). As elsewhere, these troughs, both of which host cyclonic circulations (Schulze Chretien et al., 2021; Zhang et al., 2016), appear to be the principal conduits by which mCDW transits the continental shelf and accesses the ice shelves (Ruan et al., 2021; Schulze Chretien et al., 2021). Flow in the troughs is largely barotropic (Schulze Chretien et al., 2021). Meltwater has been observed across the Bellingshausen (Zhang et al., 2016), but there is evidence that it is concentrated in the northward flowing limbs of the troughs' cyclonic gyres (Ruan et al., 2021; Schulze Chretien et al., 2021; Zhang et al., 2016). Meltwater that reaches the shelf break is thought to exit the Bellingshausen via westward-flowing shelf-break currents, although evidence for this is less certain (Thompson et al., 2020; Zhang et al., 2016). Quantifying the meltwater circulation in all limbs of the troughs' circulation at a resolution sufficient to capture the small Rossby deformation radius at high latitudes would enable a more complete understanding of the role of meltwater in driving hydrographic and circulation changes in this rapidly warming region.

Here, we use novel ocean glider observations to estimate the glacial meltwater content in, and its transport around, Belgica Trough. Unlike previous ship-based surveys, the high horizontal resolution of our observations allows us to resolve the narrow boundary currents of the trough circulation for the first time. We perform tracer release experiments using a regional model to separate the pathways taken by, and density ranges occupied by, meltwater originating from the principal ice shelves of the Bellingshausen Sea's perimeter. Given the large difference in melt rates between the region's various ice shelves (Rignot et al., 2019), investigating this question should help elucidate future changes in the hydrography of the Bellingshausen Sea, and help refine projections of how attendant circulation changes might occur.

2. Methods

We analyze temperature, salinity, optical backscatter and dive-average current (Frajka-Williams et al., 2011; Garau et al., 2011; Green et al., 2014) observations collected by a Seaglider deployed in the Bellingshausen Sea (Lee et al., 2022). The glider occupied on-shelf and cross-slope transects between 1 February and 20 March 2020; we present observations from six on-shelf transects (Figure 1b), with each transect lasting four to five days. We use the glider's temperature and salinity observations (Figure S1 in Supporting Information S1) to calculate meltwater concentration following the method of Jenkins (1999), see also Biddle et al. (2017) and Zheng et al. (2021). Characteristic core temperature and salinity values of mCDW, winter water (WW) and meltwater are defined (Table S1 in Supporting Information S1); the meltwater content of an observation is then determined by quantifying the deviation, in the direction of pure meltwater, of that observation from the mCDW-WW mixing line in temperature-salinity space (Jenkins, 1999). The total geostrophic current, comprising the glider-derived geostrophic shear and a reference velocity based on the glider's de-tided (Padman et al., 2002, 2008) dive-averaged current, is used to estimate meltwater transport. A comprehensive description of the glider observations and the meltwater calculation method is presented in Supporting Information S1.

To investigate sources and pathways of meltwater, we perform high-resolution tracer release experiments using the Massachusetts Institute of Technology general circulation model, full details of which are given by Flexas et al. (2022). The model domain, which comprises the Amundsen and Bellingshausen Seas, is derived from the global configuration (LLC1080) used by the Estimating the Circulation and Climate of the Ocean project (ECCO; Forget et al., 2015) with a horizontal grid spacing of approximately 3 km. Initial and boundary conditions are derived from a global state estimate (ECCO LLC270); surface forcing is taken from ERA5 (Hersbach et al., 2020). Outputs are given as daily means. We present a comparison of the observations and model output in Supporting Information S1.

Tracers were released at a concentration of 1 kg kg^{-1} at all grid points within the nine ice shelf cavities of the Bellingshausen Sea perimeter on the first day of each month between August 2019 and July 2020 (inclusive).

Separate tracers were released under each ice shelf in order that the resulting tracer distributions might be considered individually. Tracer concentration is not the same as meltwater concentration, which would be greatest at the ice-ocean interface. Tracer concentration more accurately represents ice shelf cavity water; while it cannot be used to quantify meltwater concentration, it is used here as a proxy for identifying meltwater pathways. We present results from the August 2019 release averaged over March 2020, that is, the time of the glider observations. We focus on tracers from the George VI and Venable ice shelf cavities.

We calculate the tracer-weighted mean density, $\overline{\sigma}$ (kg m^{-3}). We first calculate tracer mass, M (kg), in a given grid box, then calculate $\overline{\sigma}$ according to:

$$\overline{\sigma} = \int_{-H}^{0} M\sigma \; dz \Big/ \int_{-H}^{0} M \; dz, \tag{1}$$

where H is the depth of the seafloor (m) and z is depth (m). Finally, we calculate the mean of $\overline{\sigma}$ over each month.

3. Glider Observations of Meltwater and Meltwater Transport

The glider's dive-average currents (Figure 1) confirm the cyclonic gyre circulation inside Belgica Trough described by previous studies (e.g., Schulze Chretien et al., 2021). There is a narrow band of northward flow in the southwest, in the vicinity of the 500 m isobath; we interpret this as the gyre's western boundary flow. Flow is approximately eastward to the immediate south of the shelf break; and there are two jets of generally southward flow in the central and eastern Trough, in water deeper than 600 m (Figure 1b). We do not observe the putative westward flow in the south that would be necessary to close the gyre circulation, likely because the glider sections do not extend sufficiently far south to reach the coast. To the east (84°W), in the shallower water between the Belgica and Latady troughs, there is also an approximately eastward flow to the south of the shelf break (Figure 1b); this suggests that the eastward flow within the trough may be a combination of a shelf-break feature and the trough's gyre circulation.

We observe net southward meltwater transport within Belgica Trough. In the north, two cores of pronounced eastward flow transport meltwater approximately parallel to the shelf break (Figure 2a). Depth-integrated meltwater content in this northern region exceeds 0.35 m (Figure 1b, where depth-integrated meltwater content is the product of meltwater concentration and bin-thickness, summed over a profile); integrated meltwater transport is 0.67 mSv (i.e., meltwater transport integrated over all depths between 30 and 70 km along transect one; 1 mSv = 10^{-3} Sv). In the central and eastern trough, two meltwater cores, each approximately 30 km wide, flow southward (Figure 2e). Depth-integrated meltwater content in these flows is approximately 0.3 m (Figure 1b); integrated meltwater transport is 0.50 mSv (0–80 km along transect five). The principal meltwater flow in the trough's western boundary current is limited in horizontal extent, being confined to a relatively narrow (10 km) northward-flowing core in the southwest (Figures 1b and 2e). Integrated meltwater transport is 0.17 mSv (0–25 km along transect three). In the shallow region between Belgica and Latady Troughs, outside Belgica Trough's gyre circulation, meltwater concentrations are relatively low (<1 g kg^{-1}; Figures 2e and 2f). The sharp boundary between the two regimes can be seen approximately 80 km along transect five (Figure 2e). We note that the glider transects may have been too short to capture the full width of the various flows, particularly in the southwest (transect three); our observations may therefore under-estimate the total meltwater transport.

Meltwater layers in Belgica Trough are centered on different density classes in different places, and the thickness of the meltwater layer varies spatially (Figure 2). In the northern and eastern trough, meltwater is present in an approximately 200 m-thick layer centered on the 27.7 kg m^{-3} isopycnal (Figures 2a and 2e). In the western trough, meltwater is present in an approximately 100 m-thick layer centered on and immediately below the 27.6 kg m^{-3} isopycnal (Figures 2b–2d). Around the center of the trough, a similarly thin (100 m) meltwater layer is present between the 27.5 and 27.6 kg m^{-1} isopycnals (Figures 2b and 2d).

Meltwater layers in Belgica Trough may be distinguished by their turbidity. The turbidity of the thick, high-meltwater flows in the northern and central trough is indistinguishable from that of the surrounding water (Figures 2a and 2e, open arrows in Figure 1b). In contrast, meltwater in the western boundary current is more turbid than the surrounding water (Figures 2b and 2c, filled arrow in Figure 1b). We note that the vertical extent of the high-turbidity regions associated with the western meltwater flows is greater than the vertical extent of the meltwater flows themselves. This is a consequence of our choosing core temperature and salinity values of

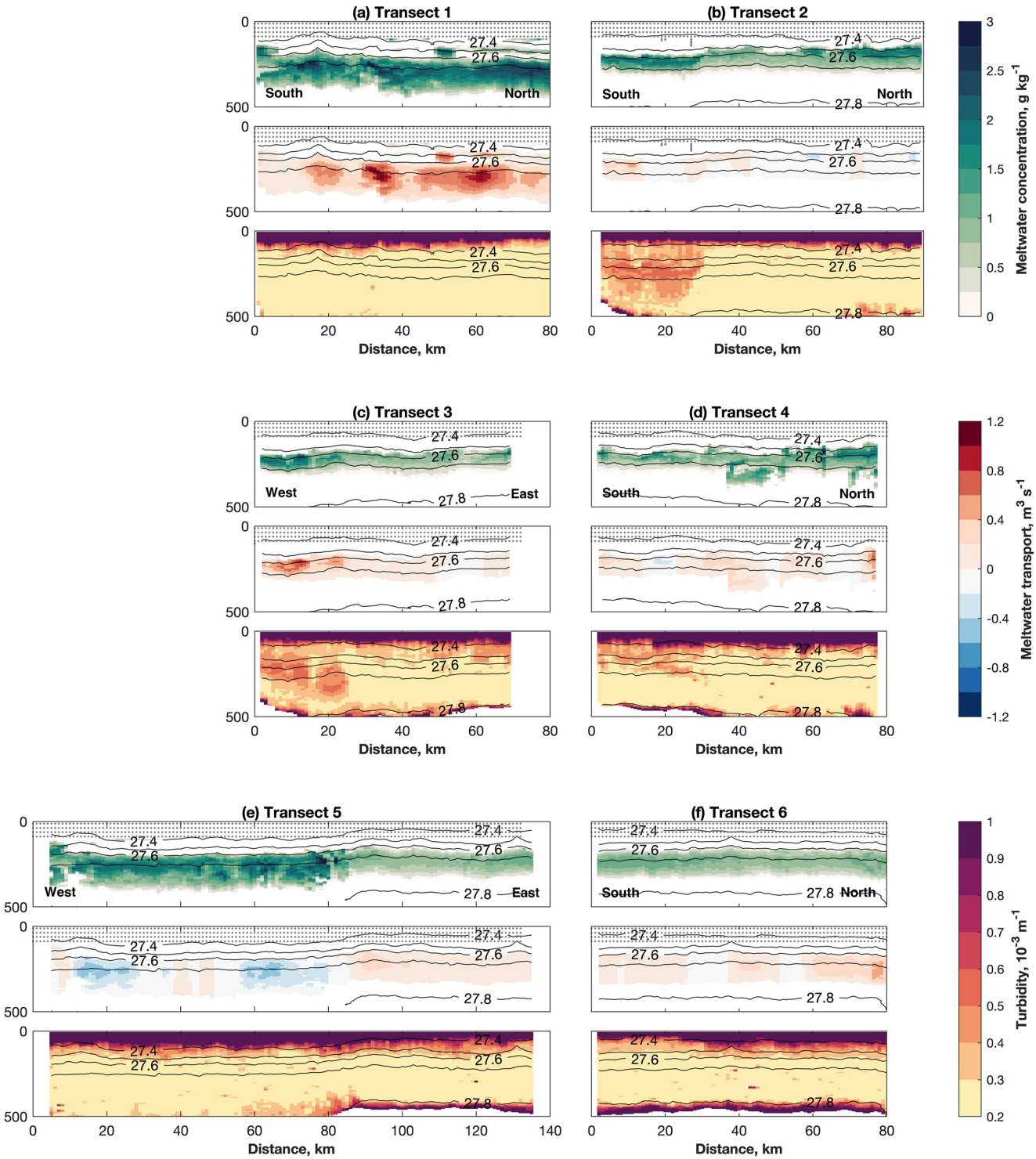

Figure 2. For each transect, top panel: meltwater concentration (g kg^{-1}); middle panel: meltwater transport (m^3 s^{-1}), where positive transport indicates northward or eastward flow; and bottom panel: turbidity (10^{-3} m^{-1}). Contours in all panels indicate potential density (kg m^{-3}). The orientation of each transect is indicated by the compass points given at each end of the top panel. Regions excluded from the meltwater calculations are indicated by the gray dots.

mCDW and WW that produce conservative estimates of meltwater. Using less conservative core temperature and salinity values of mCDW and WW (e.g., from transect three) increases the vertical extent over which meltwater is found and improves the spatial correlation between meltwater and turbidity (Figure S6 in Supporting

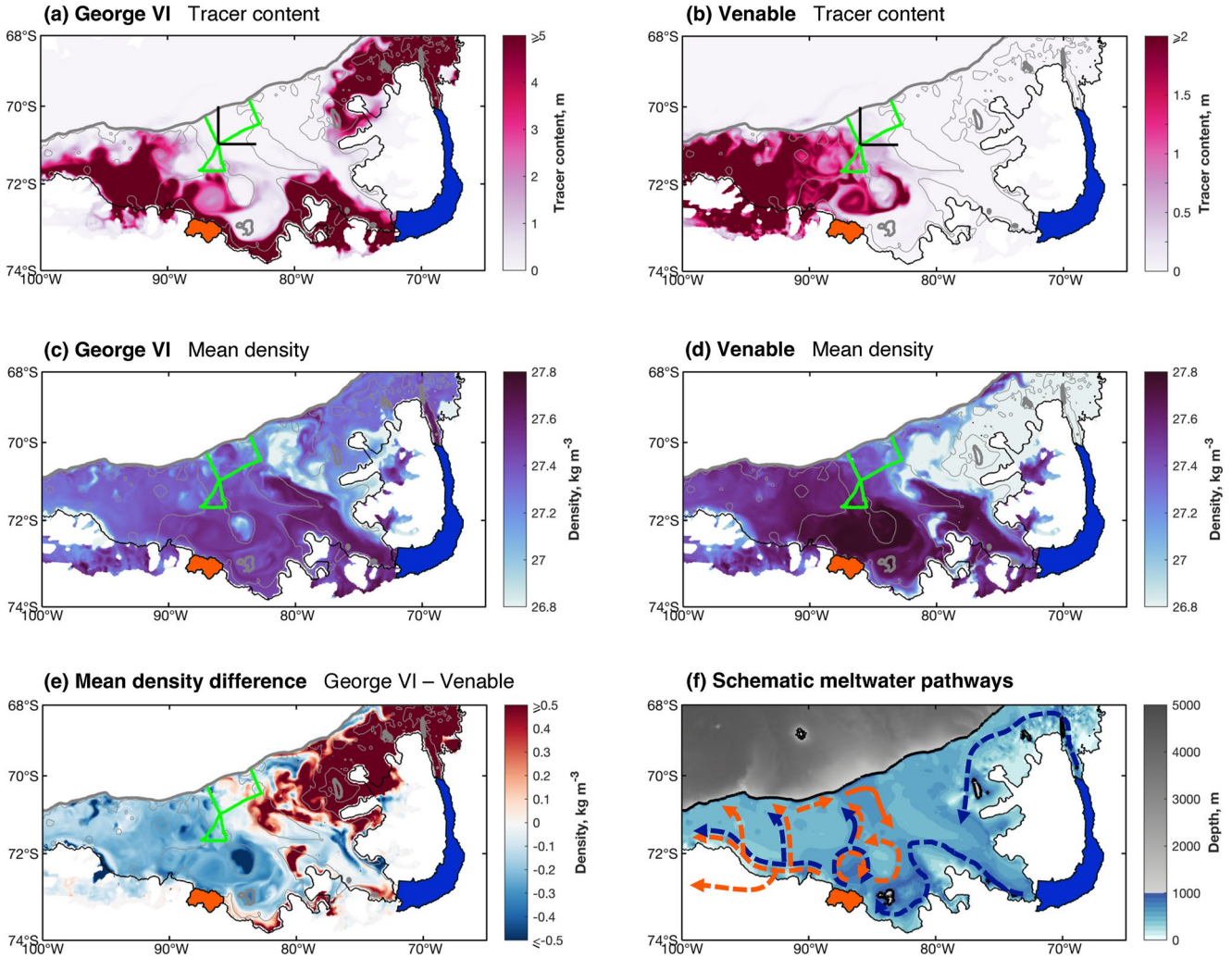

Figure 3. Depth-integrated tracer content (m) of tracers released under (a) George VI and (b) Venable; the black lines indicate the sections used to calculate tracer transport. Mean density (kg m^{-3}) of tracers released under (c) George VI and (d) Venable. (e) The difference in mean density between tracer released under George VI and Venable (George VI minus Venable). Variables in panels (a) to (e) are averages over March 2020; densities are plotted only over the continental shelf. (f) Schematic of meltwater transport pathways. Meltwater from George VI is represented by the blue arrows; meltwater from Venable is represented by the orange arrows. Regions between the 500 and 1,000 m isobaths are shaded light gray. In all panels: the ice edge is indicated by the black line and the 1,000 m isobath by the thick gray line. In panels (a) to (e), the 500 m isobath is indicated by the thin gray line and the glider path is indicated by the green line. George VI and Venable ice shelves are colored blue and orange respectively. Bathymetry is from RTopo-2.

Information S1). The distinct optical properties suggest that the two meltwater layers either originate from different ice shelves with different sediment loads, or that they originate from different locations such that their sediment load has had longer to be deposited en route.

4. Sources and Pathways of Glacial Meltwater

We turn to model simulations and tracer release experiments to investigate pathways of meltwater within the Bellingshausen, as well as the provenance of meltwater in Belgica Trough. Tracers released under both George VI and Venable ice shelves are present within the gyre circulation of Belgica Trough 7 months after release, that is, in March 2020 at the time of the glider observations (Figure 3; similarly to Figure 1b, we plot depth-integrated tracer content, i.e., the product of tracer concentration and bin-thickness, summed over a profile). Tracer released under George VI ice shelf that exits the cavity via its northern opening (70°S, 70°W) is advected southwards in the eastern Bellingshausen (Figures 3a and 3f). Tracer that exits the George VI cavity via the southern opening (73°S, 72°W) is advected westward by the Antarctic Coastal Current (Schubert et al., 2021) and is, east of 85°W,

largely confined to the coast (Figures 3a and 3f). West of approximately 90°W—that is, to the west of Belgica Trough—George VI tracer spreads northwards across the continental shelf, eventually reaching the shelf break (Figures 3a and 3f). All tracer released under Venable ice shelf is transported westward, spreading over the western Bellingshausen from the ice edge to the shelf break (Figure 3b). This generally westward tracer transport is a common feature of simulations of the Bellingshausen Sea (Dawson et al., 2023; Nakayama et al., 2014, 2017). Nakayama et al. (2014) show that, after a 10-year simulation, westward export tends to be concentrated to the south of the shelf break; in our year-long simulation, tracers first reach the western Bellingshausen in the Antarctic Coastal Current, before spreading northwards to the shelf break over the ensuing months (Figure 3 and Figure S8 in Supporting Information S1).

In the southwestern Belgica Trough, a narrow filament of tracer flows northward, toward the shelf break, in the region of the trough's western-boundary current (Figures 3a and 3b); we observe northward meltwater transport in this same feature (Figures 1 and 2c). The northward-flowing filament branches off from a small (i.e., 80–100 km across) cyclonic gyre feature immediately to the north of Venable; this Venable gyre itself draws tracer from the Antarctic Coastal Current at approximately 89°W, and tracer from both ice shelves circulates within it (Figures 3a and 3b). To the east, a second tongue branches off the Venable gyre and follows the 500 m isobath into the south-central Belgica Trough; this is particularly apparent in the distribution of the Venable tracer (Figure 3b).

Not all meltwater found in Belgica Trough flows into the trough from the south. Instead, Venable tracer flows into Belgica Trough in the northwest, having first spread over the western Bellingshausen. An eastward-flowing filament of tracer from Venable enters Belgica Trough at approximately 71°S (Figures 3b and 3f). The beginnings of such an eastward filament can be seen in tracer from George VI: this filament reaches the northern Belgica Trough in subsequent months (Figure S8 in Supporting Information S1). High meltwater concentrations and high meltwater transport are present in this eastward flow in the glider observations (Figure 2b).

Tracer from Venable is also present in the central and eastern Belgica Trough, in the region of the two cores of southward meltwater transport seen in the observations (Figures 2 and 3b and Figure S10 in Supporting Information S1). Again, tracer from George VI is absent from this region in March 2020, but is present in subsequent months (Figure S8 in Supporting Information S1). The concentration of Venable tracer in this region increases in subsequent months, and the filament penetrates further southward (Figure S8 in Supporting Information S1). As in the western Belgica Trough, tracer re-circulating in the eastern trough largely remains in waters deeper than 500 m (Figure 3d). This agrees with our observations of this southward flow (Figures 1b and 2e): meltwater concentrations are high in the southward flow within the trough, and lower outside the trough's cyclonic gyre, that is, in the shallower region between Belgica and Latady troughs.

We calculate the cumulative sum of tracer mass, as a percentage of the total mass of tracer released, that crosses: a meridional section at 86°W, between 70 and 71°S (i.e., the eastward flow in the northern Belgica trough); and a zonal section at 71°S, between 83 and 86°W (i.e., the southward re-circulation). Over the year-long simulation, 0.6% of the George VI total tracer mass crosses the meridional section, and 0.3% crosses the zonal section. Of the Venable tracer, 4.7% crosses the meridional section and 3.1% crosses the zonal section.

Tracers from George VI and Venable ice shelves predominate at different mean densities, $\overline{\sigma}$, within the Bellingshausen Sea. In the southwestern Belgica Trough, as across the western Bellingshausen, tracer from George VI is found at mean densities between approximately 27.4 and 27.6 kg m^{-3} (Figure 3c); tracer from Venable is found at greater mean densities: between approximately 27.6 and 27.8 kg m^{-3} (Figure 3d). This density difference of approximately 0.1–0.2 kg m^{-3} in the western Bellingshausen is broadly consistent over time (not shown). In both the northern and eastern Belgica Trough, the difference between the mean densities of the George VI and Venable tracers is, in places, close to zero (Figure 3e). This qualitative pattern is consistent for tracer released in all months (not shown). The fact that tracer originating under Venable is found on denser isopycnals than tracer from under George VI may explain why the former penetrates the cavities under western ice shelves such as Abbot, whereas the latter, higher in the water column, remains in open water (Figures 3a and 3b).

The mean densities of tracer from George VI, in the eastern Bellingshausen, and Venable, in the southern Bellingshausen, are representative of the mean densities of tracer released under the other ice shelf cavities of the eastern and southern Bellingshausen respectively: in Belgica Trough and across the western Bellingshausen Sea, tracer from eastern ice shelves (i.e., George VI, Wilkins and Bach) is found at lesser mean densities (i.e., shallower) than tracer from southern ice shelves (i.e., Venable and Ferrigno). This modeling result is consistent with the

difference between the density of meltwater layers that we observe in Belgica Trough. Relatively dense meltwater layers, such as that observed in the northern and western trough ($\geq$27.7 kg m^{-3}; Figures 2a and 2e) contain meltwater from southern ice shelves; relatively light meltwater layers, such as those observed in the southwestern trough ($\leq$27.6 kg m^{-3}; Figures 2b and 2c) contain meltwater from eastern ice shelves.

We may now synthesize results from the observations and the modeling experiments in a schematic of meltwater transport in the Bellingshausen Sea (Figure 3f). While the model suggests that tracers from the ice shelves of the eastern and southern Bellingshausen enter Belgica Trough in the southwest, that is, from the small gyre immediately north of Venable Ice Shelf (orange in Figure 3), we observe only lighter meltwater flowing northward in the western boundary current (Figures 2b and 2c). Consequently, we conclude that meltwater in the western boundary current originates from the eastern Bellingshausen (e.g., George VI). Furthermore, meltwater from the eastern Bellingshausen would therefore appear to be responsible for the high-turbidity signal in the observations. Meltwater observed in the northern and western Belgica Trough is present in a thicker, lighter layer, and is of low turbidity. These differences suggest a different origin to the denser, more turbid meltwater layer observed in the western Bellingshausen; the model results suggest that meltwater in the northern and western Belgica Trough originates from the southern Bellingshausen (e.g., Venable). We note that the model indicates a pathway for dense Venable meltwater via the western boundary current (Figure 2b); this is not observed, but its absence may be due to temporal variability that we miss with a single glider transect, or else due to spatially incomplete observations because the glider did not go south to the coast because of sea-ice coverage. Nevertheless, the lack of dense Venable-origin meltwater observed in the western boundary current invites speculation on an alternative pathway between Venable and the northwestern Belgica Trough: the tracer results suggest that this is via the western Bellingshausen (Figure 3). And since high-turbidity meltwater in Belgica Trough originates from further away than low turbidity-meltwater, we discount the hypothesis that the difference is due to high-turbidity meltwater having been transported further from its source, depositing its sediment load en route; rather, meltwater from different ice shelves must have different initial sediment loads. This result may have important implications for the potential injection of iron, and other micro-nutrients and tracers into the Bellingshausen.

5. Discussion and Conclusions

Small-scale gyres are common features of the Antarctic continental shelf (e.g., Zheng et al., 2022), and they create the conditions in which meltwater re-circulations can occur. Given the influence of meltwater on the strength of the shelf circulation (e.g., Thurnherr et al., 2014), retention and re-circulation have the potential to induce positive feedbacks. For instance, increased melting can strengthen the on-shelf overturning circulation via water mass transformation, but advection of meltwater also influences the on-shelf density structure that determines the horizontal geostrophic circulation (Thompson et al., 2020). Both overturning and horizontal circulations influence the delivery of mCDW to the ice front, potentially allowing for ice-shelf melt feedbacks. Furthermore, an increase in meltwater-induced stratification in southward flows, which are responsible for the delivery of mCDW to the ice-front, could suppress the upward mixing of heat out of the mCDW layer (Flexas et al., 2022); warmer mCDW would then reach the ice front. Therefore, in addition to examining the far-field transport of West Antarctic meltwater and its downstream influence (e.g., Lago & England, 2019; Silvano et al., 2018), future work should consider to the local influence of meltwater build-up within in-trough gyres. Further, we note that our simulated pathways are strongly dependent on model bathymetry. Given the relative lack of ship-based bathymetry in the Bellingshausen Sea (although instrumented seals have been used to improve coverage; Padman et al., 2010), additional meltwater pathways may exist; these pathways, and their contribution to retention and re-circulation, could usefully be re-examined in future as bathymetry products improve.

We show that meltwater originating from different ice shelves becomes neutrally buoyant at different densities: meltwater from ice shelves in the eastern Bellingshausen becomes neutrally buoyant at lighter densities than meltwater from ice shelves in the southern Bellingshausen. The average density of meltwater from George VI and Venable decreases with distance from each ice shelf (Figures 2c and 2d), consistent with its mixing predominantly with lighter waters above. We also note that, at the ice front, in the model as in reality, the draft of Venable (280 m) is deeper than the draft of George VI (65 m in the north, 165 m in the south; Morlighem et al., 2020): indeed tracer from Venable is injected at greater densities than tracer from George VI (Figures 2c and 2d). Alongside the markedly different observed turbidity signatures of meltwater originating from the ice shelves of the eastern and southern Bellingshausen this suggests that the density of a meltwater layer may point

to its origin. Observations of meltwater in cavity outflows would help determine whether, in the real ocean, the density of a meltwater layer is largely set by the density at which it exits a cavity; and observations of turbulence over the Antarctic continental shelf would help determine the importance of downstream mixing in altering the initial density of a layer.

Meltwater released by ice shelves in one region may influence the circulation of the Antarctic continental shelf in different ways to meltwater released elsewhere. The volume of meltwater released by a given ice shelf, and the corresponding change in the stratification, may alter the density at which meltwater released downstream becomes neutrally buoyant. Differences in meltwater turbidity, which we propose are indicative of differences in turbidity at the original ice shelves, suggest that biogeochemical processes influenced by meltwater may be sensitive to the ice shelf from which a given meltwater sample originates. An increase in the melt rate of one ice shelf may therefore have a different physical and biogeochemical influence on Antarctica's continental shelf seas than the same increase in the melt rate of another ice shelf. Together, this suggests that not all meltwater is created equal: a full understanding of the influence of meltwater on the Antarctic continental shelf requires a quantitative understanding of the melt rate of individual ice shelves and the subsequent transport pathways of individual meltwater layers. Furthermore, an intricate system of small-scale gyres and boundary currents over the continental shelf determines the large-scale distribution of meltwater. The resulting distribution will play a large role in determining meltwater's overall influence on the circulation, both locally and downstream. Characterization of variability in these circulation features and their impact on ocean-ice interactions remains an under-explored but important research direction.

Data Availability Statement

The Seaglider observations (Lee et al., 2022) used in this study are archived at the British Oceanographic Data Centre (bodc.ac.uk) with the https://doi.org/10.5285/ea24b8e5-b10e-68bf-e053-6c86abc06c97. MITgcm and its user manual are available at: mitgcm.org/ and the source code may be downloaded from: github.com/MITgcm/MITgcm. Information on the ECCO LLC270 ocean-ice state estimate is available at: hdl.handle.net/1721.1/119821 and instructions for its download are available at: ecco-group.org/products-ECCO-V4r4.htm. The ERA5 re-analysis is available from the ECMWF (ecmwf.int/en/forecasts/datasets/reanalysis-datasets/era5), and instructions for its download are available at: confluence.ecmwf.int/display/CKB/How+to+download+ERA5. ERA5 hourly re-analysis output is also archived at the Copernicus Climate Data Store (data.marine.copernicus.eu/products) under the https://doi.org/10.24381/cds.adbb2d47 (for single-level variables) and https://doi.org/10.24381/cds.bd0915c6 (for multi-level variables). The WAIS 1080 model set-up, as well as an explanation of how to set up the tracer release experiments, is available at https://doi.org/10.5281/zenodo.6842019. RTopo-2 bathymetry (Schaffer & Timmermann, 2016) is available from Pangaea (www.pangaea.de) with the https://doi.org/10.1594/PANGAEA.856844. Data processing and figure preparation were carried out using Matlab R2021a.

Acknowledgments

PMFS and KJH were supported by the COMPASS project (Grant 741120), which was funded by the European Research Council under the Horizon 2020 program. AFT and MMF were supported by NSF award OPP-1644172 and NASA Jet Propulsion Laboratory's Research and Technical Development Earth 2050 project. The work of MPS was carried out at the Jet Propulsion Laboratory under a contract with NASA. We gratefully acknowledge support from the NASA Cryospheric Sciences Program. High-end computing resources were provided by the NASA Advanced Supercomputing Division of the Ames Research Center.

References

Biddle, L. C., Heywood, K. J., Kaiser, J., & Jenkins, A. (2017). Glacial meltwater identification in the Amundsen Sea. *Journal of Physical Oceanography*, *47*(4), 933–954. https://doi.org/10.1175/jpo-d-16-0221.1

Dawson, H. R. S., Morrison, A. K., England, M. L., & Tamsitt, V. (2023). Pathways and timescales of connectivity around the Antarctic continental shelf. *Journal of Geophysical Research: Oceans*, *128*(2), e2022JC018962. https://doi.org/10.1029/2022jc018962

Donat-Magnin, M., Jourdain, N. C., Spence, P., Le Sommer, J., Gallée, H., & Durand, G. (2017). Ice-shelf melt response to changing winds and glacier dynamics in the Amundsen Sea sector, Antarctica. *Journal of Geophysical Research: Oceans*, *122*(12), 10206–10224. https://doi.org/10.1002/2017jc013059

Flexas, M. M., Thompson, A. F., Schodlok, M. P., Zhang, H., & Speer, K. (2022). Antarctic Peninsula warming triggers enhanced basal melt rates throughout West Antarctica. *Science Advances*, *8*(32), eabj9134. https://doi.org/10.1126/sciadv.abj9134

Forget, G., Campin, J. M., Heimbach, P., Hill, C. N., Ponte, R. M., & Wunsch, C. (2015). ECCO version 4: An integrated framework for non-linear inverse modelling and global ocean state estimation. *Geoscientific Model Development*, *8*(10), 3071–3104. https://doi.org/10.5194/gmd-8-3071-2015

Frajka-Williams, E., Eriksen, C. C., Rhines, P. B., & Harcourt, R. R. (2011). Determining vertical water velocities from Seaglider. *Journal of Atmospheric and Oceanic Technology*, *28*(12), 1641–1656. https://doi.org/10.1175/2011jtecho830.1

Garau, B., Ruiz, S., Zhang, W. G., Pascual, A., Heslop, E., Kerfoot, J., & Tintoré, J. (2011). Thermal lag correction on Slocum CTD glider data. *Journal of Atmospheric and Oceanic Technology*, *28*(9), 1065–1071. https://doi.org/10.1175/jtech-d-10-05030.1

Green, R. E., Bower, A. S., & Lugo-Fernández, A. (2014). First autonomous bio-optical profiling float in the Gulf of Mexico reveals dynamic biogeochemistry in deep waters. *PLoS One*, *9*(7), e101658. https://doi.org/10.1371/journal.pone.0101658

Gunn, K. L., White, N. J., Larter, R. D., & Caulfield, C. P. (2018). Calibrated seismic imaging of eddy-dominated warm-water transport across the Bellingshausen Sea, Southern Ocean. *Journal of Geophysical Research: Oceans*, *123*(4), 3072–3099. https://doi.org/10.1029/2018jc013833

Hersbach, H., Bell, B., Berrisford, P., Hirahara, S., Horányi, A., Muñoz-Sabeter, J., et al. (2020). The ERA5 global re-analysis. *Quarterly Journal of the Royal Meteorological Society*, *146*(730), 1999–2049. https://doi.org/10.1002/qj.3803

Jacobs, S. S., & Giulivi, C. F. (2010). Large multidecadal salinity trends near the Pacific-Antarctic continental margin. *Journal of Climate*, *23*(17), 4508–4524. https://doi.org/10.1175/2010jcli3284.1

Jenkins, A. (1999). The impact of melting ice on ocean waters. *Journal of Physical Oceanography*, *29*(9), 2370–2381. https://doi.org/10.1175/1520-0485(1999)029<2370:tiomio>2.0.co;2

Jenkins, A., & Jacobs, S. (2008). Circulation and melting beneath George VI ice shelf, Antarctica. *Journal of Geophysical Research*, *113*(C4), C04013. https://doi.org/10.1029/2007jc004449

Jenkins, A., Shoosmith, D., Dutrieux, P., Jacobs, S., Kim, T. W., Lee, S. H., et al. (2018). West Antarctic ice sheet retreat in the Amundsen Sea driven by decadal oceanic variability. *Nature Geoscience*, *11*(10), 733–738. https://doi.org/10.1038/s41561-018-0207-4

Kim, T.-W., Yang, H. W., Dutrieux, P., Wåhlin, A. K., Jenkins, A., Kim, Y. G., et al. (2021). Interannual variation of modified circumpolar deep water in the Dtoson-Getz Trough, West Antarctica. *Journal of Geophysical Research: Oceans*, *126*, e2021JC017491. https://doi.org/10.1029/2021JC017491

Kimura, S., Jenkins, A., Regan, H., Holland, P. R., Assmann, K. M., Whitt, D. B., et al. (2017). Oceanographic controls on the variability of ice-shelf basal melting and circulation of glacial meltwater in the Amundsen Sea Embayment, Antarctica. *Journal of Geophysical Research: Oceans*, *122*(12), 10131–10155. https://doi.org/10.1002/2017jc012926

Lago, V., & England, M. L. (2019). Projected slowdown of Antarctic Bottom Water in response to amplified meltwater contributions. *Journal of Climate*, *32*(19), 6319–6335. https://doi.org/10.1175/jcli-d-18-0622.1

Lee, G. A., Damerell, G. M., Heywood, K. J., Oelerich, R., Azaneu, M., Flexas, M. M., et al. (2022). *Seaglider observations in the Belgica Trough and over the continental slope of the Bellingshausen Sea, Antarctica, February to March 2020*. British Oceanographic Data Centre, National Oceanography Centre. Retrieved from www.bodc.ac.uk/data/published_data_library/catalogue/10.5285/ea24b8e5-b10e-68bf-e053-6c86abc06c97/

Moffat, C., Owens, B., & Beardsley, R. C. (2009). On the characteristics of Circumpolar Deep Water intrusions to the west Antarctic Peninsula continental shelf. *Journal of Geophysical Research*, *114*(C5), C05017. https://doi.org/10.1029/2008jc004955

Morlighem, M., Rignot, E., Binder, T., Blankenship, D., Drews, R., Eagles, G., et al. (2020). Deep glacial troughs and stabilising ridges unveiled beneath the margins of the Antarctic ice sheet. *Nature Geoscience*, *13*(2), 132–137. https://doi.org/10.1038/s41561-019-0510-8

Nakayama, Y., Menemenlis, D., Schodlok, M., & Rignot, E. (2017). Amundsen and Bellingshausen Seas simulation with optimised ocean, sea ice and thermodynamic ice shelf model parameters. *Journal of Geophysical Research: Oceans*, *122*(8), 6180–6195. https://doi.org/10.1002/2016jc012538

Nakayama, Y., Menemenlis, D., Zhang, H., Schodlok, M., & Rignot, E. (2018). Origin of circumpolar deep water intruding onto the Amundsen and Bellingshausen Sea continental shelves. *Nature Communications*, *9*(1), 3403. https://doi.org/10.1038/s41467-018-05813-1

Nakayama, Y., Timmermann, R., & Hellmer, H. H. (2020). Impact of West Antarctic ice shelf melting on Southern Ocean hydrography. *The Cryosphere*, *14*(7), 2205–2216. https://doi.org/10.5194/tc-14-2205-2020

Nakayama, Y., Timmermann, R., Rodehacke, C. B., Schröder, M., & Hellmer, H. H. (2014). Modelling the spreading of glacial meltwater from the Amundsen and Bellingshausen Seas. *Geophysical Research Letters*, *41*(22), 7942–7949. https://doi.org/10.1002/2014gl061600

Oelerich, R., Heywood, K. J., Damerell, G. M., & Thompson, A. F. (2022). Wind-induced variability of warm water on the southern Bellingshausen Sea continental shelf. *Journal of Geophysical Research: Oceans*, *127*(11), e2022JC018636. https://doi.org/10.1029/2022jc018636

Orsi, A. H., Whitworth, T., & Nowlin Jnr, W. D. (1995). On the meridional extent and fronts on the Antarctic Circumpolar Current. *Deep-Sea Research I*, *42*(5), 641–673. https://doi.org/10.1016/0967-0637(95)00021-w

Padman, L. H., Costa, D. P., Bolmer, S. T., Goebel, M. E., Huckstadt, L. A., Jenkins, A., et al. (2010). Seals map bathymetry of the Antarctic continental shelf. *Geophysical Research Letters*, *37*(21), L21601. https://doi.org/10.1029/2010gl044921

Padman, L. H., Erofeeva, S. Y., & Fricker, H. A. (2008). Improving Antarctic tide models by assimilation of ICESat laser altimetry over ice shelves. *Geophysical Research Letters*, *35*(22), L22504. https://doi.org/10.1029/2008gl035592

Padman, L. H., Fricker, H. A., Coleman, R., Howard, S., & Erofeeva, S. Y. (2002). A new tide model for the Antarctic ice shelves and seas. *Annals of Glaciology*, *34*, 247–254. https://doi.org/10.3189/172756402781817752

Rignot, E., Mouginot, J., Scheuchl, B., van den Broeke, M., van Wessem, M. J., & Morlighem, M. (2019). Four decades of Antarctic ice sheet mass balance from 1979 to 2017. *Proceedings of the National Academy of Sciences of the United States of America*, *116*(4), 1095–1103. https://doi.org/10.1073/pnas.1812883116

Ruan, X., Speer, K. G., Thompson, A. F., Schulze Chretien, L. M., & Shoosmith, D. R. (2021). Ice-shelf meltwater overturning in the Bellingshausen Sea. *Journal of Geophysical Research: Oceans*, *126*(5), e2020JC016957. https://doi.org/10.1029/2020jc016957

Schaffer, J., & Timmermann, R. (2016). *Greenland and Antarctic ice sheet topography, cavity geometry and global bathymetry, (Rtopo-2)*. Pangaea. https://doi.org/10.1594/PANGAEA.856844

Schubert, R., Thompson, A. F., Speer, K., Schulze Chretien, L., & Bebieva, Y. (2021). The Antarctic coastal current in the Bellingshausen Sea. *The Cryosphere*, *15*(9), 4179–4199. https://doi.org/10.5194/tc-15-4179-2021

Schulze Chretien, L. M., Thompson, A. F., Flexas, M. M., Speer, K., Swaim, N., Oelerich, R., et al. (2021). The shelf circulation of the Bellingshausen Sea. *Journal of Geophysical Research: Oceans*, *126*(5), e2020JC016871. https://doi.org/10.1029/2020jc016871

Silvano, A., Rintoul, S. R., Peña-Molino, B., Hobbs, W. R., van Wijk, E., Aoki, S., et al. (2018). Freshening by glacial meltwater enhances melting of ice shelves and reduces formation of Antarctic Bottom Water. *Science Advances*, *4*, eaap9467. https://doi.org/10.1126/sciadv.aap9467

Thompson, A. F., Speer, K. G., & Schulze Chretien, L. M. (2020). Genesis of the Antarctic slope current in west Antarctica. *Geophysical Research Letters*, *47*(16), e2020GL087802. https://doi.org/10.1029/2020gl087802

Thompson, A. F., Stewart, A. L., Spence, P., & Heywood, K. J. (2018). The Antarctic Slope Current in a changing climate. *Reviews of Geophysics*, *56*(4), 741–770. https://doi.org/10.1029/2018rg000624

Thurnherr, A. M., Jacobs, S. S., Dutrieux, P., & Giulivi, C. F. (2014). Export and circulation of ice cavity water in Pine Island Bay, west Antarctica. *Journal of Geophysical Research: Oceans*, *119*(3), 1754–1764. https://doi.org/10.1002/2013jc009307

Wåhlin, A. K., Yuan, X., Björk, G., & Nohr, C. (2010). Inflow of warm circumpolar deep water in the central Amundsen shelf. *Journal of Physical Oceanography*, *40*(6), 1427–1434. https://doi.org/10.1175/2010jpo4431.1

Whitworth, T., Orsi, A. H., Kim, S.-J., Nowlin, W. D., & Locarnini, R. A. (1998). Water masses and mixing near the Antarctic Slope Front. In S. J. Jacobs & F. Weiss (Eds.), *Ocean, ice, and atmosphere: Interactions at the Antarctic continental margin* (pp. 1–27). United States of America: American Geophysical Union.

Zhang, X., Thompson, A. F., Flexas, M. M., Roquet, F., & Bornemann, H. (2016). Circulation meltwater distribution in the Bellingshausen Sea: From shelf break to coast. *Geophysical Research Letters*, *43*(12), 6402–6409. https://doi.org/10.1002/2016gl068998

Zheng, Y., Heywood, K. J., Webber, B. G. M., Stevens, D. P., Biddle, L. C., Boehme, L., & Loose, B. (2021). Winter seal-based observations reveal glacial meltwater surfacing in the southeastern Amundsen Sea. *Communications Earth & Environment*, *2*(1), 40. https://doi.org/10.1038/s43247-021-00111-z

Zheng, Y., Stevens, D. P., Heywood, K. J., Webber, B. G. M., & Queste, B. Y. (2022). Reversal of ocean gyres near ice shelves in the Amundsen Sea caused by the interaction of sea ice and wind. *The Cryosphere*, *16*(7), 3005–3019. https://doi.org/10.5194/tc-16-3005-2022